

## Low-frequency Raman scattering from CdS microcrystals embedded in a germanium dioxide glass matrix

Akinori Tanaka, Seinosuke Onari, and Toshihiro Arai

*Institute of Applied Physics, University of Tsukuba, Tsukuba, Ibaraki 305, Japan*

(Received 11 February 1992; revised manuscript received 11 May 1992)

We report here results from experiments on low-frequency Raman scattering from CdS microcrystals of various sizes embedded in a germanium dioxide glass matrix. We observed peaks in the low-frequency region in the tail parts of the Rayleigh lines and we found that the frequencies of these peaks were proportional to the inverse microcrystal diameters and that the size dependences of the peak shifts agreed fairly well with the calculated results based on Lamb's theory. Furthermore, we found that these Raman-scattering spectra had the characteristic polarization properties. Our results show that the observed low-frequency Raman scattering originates from confined acoustic vibrations of a spherical CdS microcrystal.

### I. INTRODUCTION

Optical properties of semiconductor microcrystals are recently attracting much interest because they are expected to differ strongly from those of the corresponding bulk crystals. Especially from the viewpoint of applying them as optical processing devices, semiconductor microcrystals embedded in solid matrices, such as NaCl single crystals,<sup>1,2</sup> and GeO<sub>2</sub> (Refs. 3 and 4) and SiO<sub>2</sub> glasses,<sup>5-10</sup> have been investigated extensively. In a small microcrystal with a size in the range of a few nanometers to several tens of nanometers, zero-dimensional confinement effects on electron-hole systems (quantum size effects) become predominant. Due to these effects, distinct physical properties (electronic states, carrier dynamics, and optical nonlinear susceptibility, etc.) appear that have been studied experimentally<sup>1-10</sup> and theoretically.<sup>11-17</sup> Furthermore, in order to elucidate the optical properties of semiconductor microcrystals, it is indispensable to consider the zero-dimensional confinement effects on phonons as well as on electron-hole pairs (excitons), and to discuss the electron-phonon interactions in a microcrystal. The investigation of Raman scattering is one of the important methods used to obtain information on vibrational states. In addition, the investigation of Raman scattering is the effective method used to appraise the microcrystal samples, because the Raman scattering of the microcrystal is sensitively influenced by the condition of the surface (the presence of disordered interfacial regions and the presence of stress on the microcrystal's surface, etc.). Up to now, by the observation of Raman scattering of semiconductor microcrystals, several researchers discussed the zero-dimensional confinement effect of optical phonons,<sup>18-23</sup> the surface phonon mode,<sup>24-26</sup> and the presence of disordered interfacial regions for evaporated microcrystals in an inert gas.<sup>27-29</sup>

Recently, low-frequency Raman scattering by nucleated glass containing MgCr<sub>2</sub>O<sub>4</sub>-MgAlO<sub>4</sub> microcrystals was first reported by Duval, Boukenter, and Champagnon.<sup>30</sup> They observed the appearance of a distinct Raman band

in the low-frequency region of 5–20 cm<sup>-1</sup>. From a comparison of these data with the theoretical eigenfrequencies, they concluded that the Raman bands could be considered to be due to the confined acoustic-phonon modes in microcrystals. In particular, they showed that the surface modes among the confined acoustic vibrations were responsible for this low-frequency Raman scattering. After that, similar low-frequency Raman-scattering spectra for nucleated glass,<sup>31</sup> Ge microcrystals embedded in GeO<sub>2</sub> glass,<sup>32</sup> Ag microcrystals embedded in alkali halide (NaCl, KI),<sup>33</sup> and Ag microcrystals embedded in SiO<sub>2</sub> glass<sup>34</sup> were reported by several researchers.

In this paper, we will report results from low-frequency Raman-scattering measurements on CdS microcrystals embedded in a germanium dioxide glass matrix. We observed peaks in the low-frequency region in the tail parts of the Rayleigh line, and we found that the peak frequencies were proportional to the inverse microcrystal diameters,  $1/d$ . From a comparison of our experimental results with results of a calculation based on Lamb's theory, which deals with the free vibrations of a homogeneous spherical elastic body, we conclude that the observed low-frequency Raman scattering originates from the localized acoustic-phonon mode of a spherical CdS microcrystal. In the previous papers,<sup>30-34</sup> the specific polarization properties of these low-frequency Raman bands have not been observed, and only the surface modes (the lowest-frequency modes) have been observed. In this report, we succeeded in observing specific polarization properties, and we discuss the Raman bands due to the inner modes (the higher-frequency modes).

### II. EXPERIMENT

The samples were prepared using two processes. The first process was a synthesis of base glasses doped with Cd and S atoms and/or ions as a supersaturated solid solution. The host glasses were GeO<sub>2</sub> containing soda in the form of Na<sub>2</sub>GeO<sub>3</sub>. The molar ratio of GeO<sub>2</sub> and Na<sub>2</sub>O was 92:8. The reason for mixing soda was to lower

the heat-treatment temperature. Cd powder of 0.9 mol. % and S powder of 2.59 mol. % were mixed to the glassy powder described above. They were then sealed in an evacuated double-covered quartz ampoule at  $10^{-4}$  Pa. The ampoule was heated gradually up to  $1180^{\circ}\text{C}$  and rocked for 6 h in order to disperse Cd and S atoms and/or ions in a glassy matrix homogeneously. Subsequently, they were quenched in air down to room temperature, and the base glasses were obtained. The second process was the thermal annealing of the base glasses doped with Cd and S atoms and/or ions for the growth of CdS microcrystals in a glassy matrix. The base glasses were annealed for various periods of time (10–60 min) at various temperatures ( $550$ – $650^{\circ}\text{C}$ ) in air. The size of CdS microcrystals was controlled by a change of the annealing conditions. The average size of the grown CdS microcrystals was estimated both by direct observation with a transmission electron microscope (JEM 200CX) operated at 200 kV and by applying the theoretical results of Kayanuma<sup>14</sup> on the modified lowest-excited-state energy due to quantum confinement effects on the observed absorption edge in absorption spectra and in photoacoustic spectra. The diameter  $d$  of synthesized CdS microcrystals used in this experiment was in the range 7–25 nm.

For the Raman-scattering measurement, we used the 514.5-nm line of an argon ion laser (N.E.C. GLS3260J) as the exciting light along with a double-pass monochromator (Jobin Yvon U-1000). The spectra were recorded by a photon-counting system equipped with a photomultiplier (RCA C31034) and a multichannel analyzer (Canberra Series 40). The measurements were made in backscattering geometry using a cylindrical lens for focusing the laser beam on the sample surface, and the excitation power of the argon ion laser at the sample was set to be less than about 5 mW to avoid the local heating of the sample. No change in the optical properties due to laser irradiation was observed under the conditions of our measurements. To investigate polarization features, we observed polarized scattering spectra in the HH geometry (the electric-field vector of the scattered light was parallel to that of the exciting light) as well as depolarized scattering spectra in the HV geometry (the electric-field vector of the scattered light was perpendicular to that of the exciting light). The shape of the sample used in the Raman-scattering measurement was a platelet with a thickness of about  $500\ \mu\text{m}$ . All our measurements were carried out at room temperature.

### III. RESULTS

Figures 1 and 2 show the low-frequency Raman-scattering spectra we obtained at room temperature for CdS microcrystals of various sizes embedded in a  $\text{GeO}_2$  glass matrix. Figure 1 shows the polarized scattering spectra measured in the HH geometry, and Fig. 2 shows the depolarized scattering spectra measured in the HV geometry. In the polarized scattering spectra, as shown in Fig. 1, no structure was observed in the low-frequency

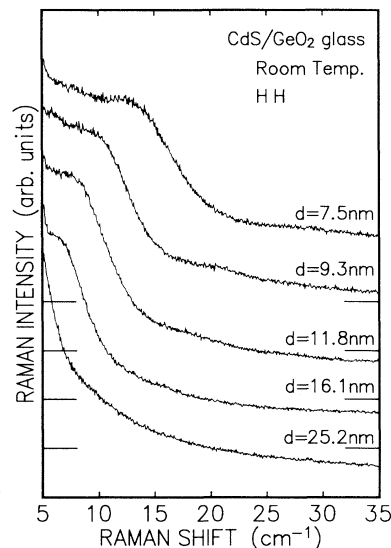


FIG. 1. Size dependence of the low-frequency polarized Raman-scattering spectra measured for CdS microcrystals embedded in a germanium dioxide glass matrix.

region for the sample with  $d=25.2$  nm; however, a shoulder could be observed at about  $7\ \text{cm}^{-1}$  for the sample with  $d=16.1$  nm. As the size of the microcrystals decreased, a distinct shoulder appeared gradually and could be observed at about  $14\ \text{cm}^{-1}$  for the sample with  $d=7.5$  nm. These shoulders seemed to shift to the higher-frequency side with decreasing microcrystal size. In the depolarized scattering spectra, as shown in Fig. 2, the structure that was confirmed in the polarized scattering spectra could not be observed in the measured low-

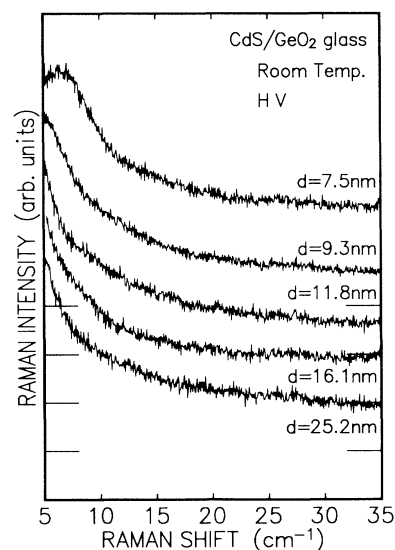


FIG. 2. Size dependence of the low-frequency depolarized Raman-scattering spectra measured for CdS microcrystals embedded in a germanium dioxide glass matrix.

frequency region for the samples with  $d=25.2$ , 16.1, 11.8, and 9.3 nm. However, a distinct peak could be confirmed at about  $7 \text{ cm}^{-1}$  for the sample with  $d=7.5 \text{ nm}$ . In the depolarized scattering spectra, the low-frequency Raman peak appeared only for the sample with  $d=7.5 \text{ nm}$ .

When dealing with low-frequency Raman scattering in disordered systems, the analysis should be performed on the reduced Raman intensity,  $I_r = I/[n(\omega)+1]$ , where  $n(\omega)$  is the Bose-Einstein occupation factor and  $I$  is the observed Raman intensity. Figures 3 and 4 show the reduced Raman-scattering spectra for polarized and depolarized scattering (corresponding to Figs. 1 and 2), respectively. The observed Raman scattering spectra in the HH geometry exhibited shoulderlike spectra as shown in Fig. 1; however, distinct peaks were obtained in the reduced spectra as shown in Fig. 3. These distinct peaks corresponded to the shoulder structure of the observed spectra in the HH geometry. In the reduced spectra of polarized scattering, the tail part of a peak was observed at about  $5\text{--}7 \text{ cm}^{-1}$  for the sample with  $d=25.2 \text{ nm}$ , and the peaks shifted to the higher-frequency side with decreasing microcrystal size. As shown in Fig. 4, in the reduced spectra of depolarized scattering, the distinct peak could not be confirmed for the samples with  $d=25.2$ , 16.1, 11.8, and 9.3 nm, but a distinct peak could be confirmed for the sample with 7.5 nm. These results corresponded to the results of the observed Raman spectra (Fig. 2). In order to see more clearly the size dependence of the peak frequencies of these Raman bands, the peak frequencies are plotted as functions of the inverse microcrystal size in Figs. 5(a) and 5(b). Here, we assumed that the reduced polarized scattering spectra for the samples with  $d=9.3$  and 7.5 nm were composed of two peaks, and we performed a decomposition of the peaks. As shown in Fig. 5, we found that the peak frequency is proportional to the inverse microcrystal diameter.

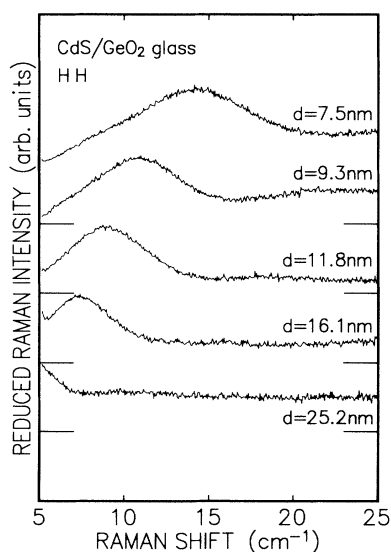


FIG. 3. Size dependence of the reduced polarized Raman-scattering spectra by the Bose-Einstein occupation factor.

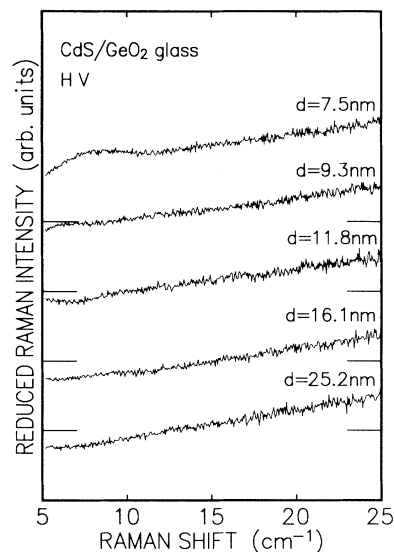


FIG. 4. Size dependence of the reduced depolarized Raman-scattering spectra by the Bose-Einstein occupation factor.

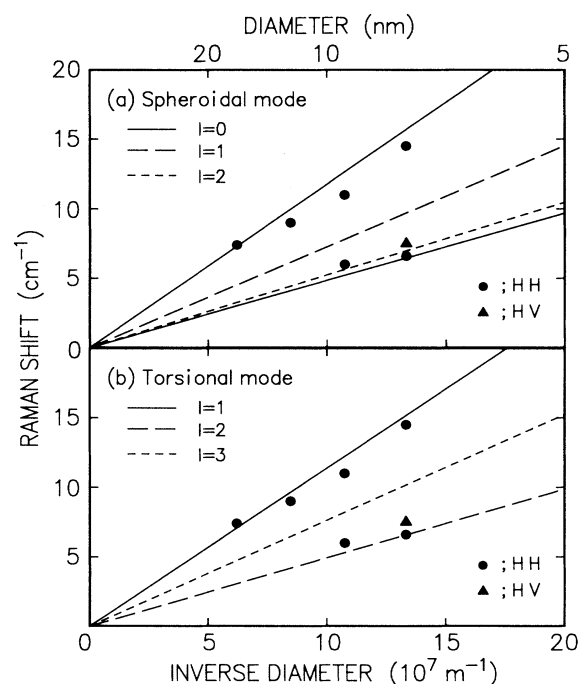


FIG. 5 Plot of the peak wave numbers obtained from the reduced polarized spectra (solid circles) and the peak wave number obtained from the reduced depolarized spectrum (solid triangle) as a function of the inverse microcrystal diameter. In (a), the solid lines, the dashed line, and the dotted line represent the Raman-shift wave numbers of  $l=0$  spheroidal modes [Eq. (6)], that of the  $l=1$  spheroidal mode [Eq. (7)] and that of the  $l=2$  spheroidal mode [Eq. (8)], respectively. In (b), the solid line, the dashed line, and the dotted line represent the Raman-shift wave numbers of the  $l=1$  torsional mode [Eq. (10)], that of the  $l=2$  torsional mode [Eq. (11)], and that of the  $l=3$  torsional mode [Eq. (12)], respectively.

#### IV. DISCUSSION

##### A. Review of previous experimental results

Low-frequency Raman-scattering spectra for nucleated glass containing microcrystals was first observed by Duvall, Boukenter, and Champagnon.<sup>30</sup> In their report, the additional Raman bands that appeared in the low-frequency region were considered to be due to an elastic vibration of the microcrystal itself, that is, to the confined acoustic-phonon mode in a spherical microcrystal, as we shall describe below. From a comparison with the theoretical eigenfrequencies calculated from the theory of Lamb,<sup>35</sup> to be described here later, they found that the frequencies of these observed Raman bands agreed with the calculated lowest-frequency mode. Because the lowest-frequency modes have large amplitudes at the surface of the microcrystal and are defined as the surface modes, they concluded that the surface modes among the confined acoustic modes of microcrystals were responsible for these low-frequency Raman scatterings. Similar low-frequency Raman-scattering spectra for nucleated glass,<sup>31</sup> Ge microcrystals embedded in GeO<sub>2</sub> glass,<sup>32</sup> Ag microcrystals embedded in alkali halide (NaCl, KI) crystals,<sup>33</sup> and Ag microcrystals embedded in SiO<sub>2</sub> glass<sup>34</sup> were reported by several researchers. In these latter reports,<sup>30-34</sup> the lowest-frequency modes (the surface modes) have been observed, but the higher-frequency modes (the inner modes) have not been observed. Furthermore, specific polarization properties have not been reported in the previous papers. In our experiment, however, we observed the specific polarization properties of low-frequency Raman scattering from the embedded microcrystals and we shall report them here. To explain

$$2 \left[ \eta^2 + (l-1)(l+2) \left( \frac{\eta j_{l+1}(\eta)}{j_l(\eta)} - (l+1) \right) \right] \frac{\xi j_{l+1}(\xi)}{j_l(\xi)} - \frac{1}{2} \eta^4 + (l-1)(2l+1)\eta^2 + \{ \eta^2 - 2l(l-1)(l+2) \} \frac{\eta j_{l+1}(\eta)}{j_l(\eta)} = 0 \quad \text{for } l \geq 0, \quad (2)$$

where  $\xi$  and  $\eta$  are dimensionless eigenvalues, and  $j_l(\eta)$  is the spherical Bessel function of first kind. The spheroidal mode is derived from both the scalar and vector potentials, and their eigenvalues depend on the materials through the ratio  $v_l/v_t$ , where  $v_l$  is the longitudinal sound velocity, and  $v_t$  is the transverse sound velocity. This will be discussed in detail in a later section of this work. The eigenvalues  $\xi_l^S$  and  $\eta_l^S$  are written as follows:

$$\xi_l^S = \frac{\omega_l^S d}{2v_l}, \quad \eta_l^S = \frac{\omega_l^S d}{2v_t}, \quad (3)$$

where  $\omega_l^S$  is the angular frequency characterized by the angular momentum quantum number  $l$ , and  $d$  is the diameter of the microcrystal. The torsional mode is a vibration without dilatation, and its eigenvalue equation is given by

$$j_{l+1}(\eta) - \frac{l-1}{\eta} j_l(\eta) = 0 \quad \text{for } l \geq 1. \quad (4)$$

our experimental data, we will discuss the low-frequency Raman-scattering feature of the confined acoustic vibration of the small spherical microcrystal, itself.

##### B. Lamb's theory and its application to the present experiment

A long-wavelength acoustic phonon that propagates in an ideal bulk crystal is usually described by the vibrational theory of a continuous elastic body. If we want to discuss a confined acoustic phonon in a small microcrystal, we need to consider the boundary condition on the surface of the microcrystal in addition to the usual vibrational theory of the elastic body. At the end of the last century, Lamb theoretically discussed the free vibrations of a homogeneous elastic body of spherical shape under stress-free boundary conditions.<sup>35</sup> In other words, Lamb's theory deals with the confined acoustic phonon in a small spherical volume. Tamura and co-workers<sup>36,37</sup> and Nishiguchi and Sakuma<sup>38</sup> have recently extended Lamb's theory.

Lamb's theory begins with the equation of motion of a three-dimensional elastic body:

$$\rho \partial^2 \mathbf{D} / \partial t^2 = (\lambda + \mu) \nabla(\nabla \cdot \mathbf{D}) + \mu \nabla^2 \mathbf{D}, \quad (1)$$

where  $\mathbf{D}$  is the displacement vector, the two parameters  $\lambda$  and  $\mu$  are Lamé's constants, and  $\rho$  is the mass density. Under stress-free boundary conditions, Eq (1) can be solved by introducing a scalar potential and a vector potential. In this way, Lamb obtained two types of vibrational modes: a spheroidal mode and a torsional mode. The spheroidal mode is a vibration with dilatation, and its eigenvalue equation is given by

It should be mentioned that the displacement of the torsional mode is defined for  $l \geq 1$  because the torsional mode of  $l=0$  has null displacement. The eigenvalue  $\eta_l^T$  is written as follows:

$$\eta_l^T = \frac{\omega_l^T d}{2v_t}. \quad (5)$$

Unlike in the case of the spheroidal mode, in the present case the eigenvalues do not depend on the materials because the torsional mode is derived only from the vector potential and its eigenvalues depend only on the transverse sound velocity  $v_t$ .

The eigenvalues of the torsional mode have been reported already<sup>35-38</sup> because they do not depend on the materials. However, the eigenvalues of the spheroidal mode depend on the materials. With the sound velocities of CdS ( $v_l = 4247$  m/sec and  $v_t = 1859$  m/sec) reported by Gerlich,<sup>39</sup> the eigenvalues of the spheroidal mode in this

case of CdS microcrystal can be calculated from Eq. (2). Figure 6 shows the calculated values of  $\eta_{nl}^S$  and  $\eta_{nl}^T$  for  $l \leq 3$  that were obtained by solving Eqs. (2) and (4), respectively. The vibrational eigenfrequencies  $\eta_{nl}^S$  and  $\eta_{nl}^T$  are specified by two state variables: an angular momentum  $l$  and a branch number  $n$ . Both  $\eta_{nl}^S$  and  $\eta_{nl}^T$  are the  $(n+1)$ th eigenvalues belonging to the angular momentum  $l$ . Only the lowest eigenfrequency modes with  $n=0$  in the spheroidal mode and  $n=0$  in the torsional mode correspond to the surface modes because these modes have large amplitudes near the surface of the microcrystal. The higher eigenfrequency modes of  $n \geq 1$  corresponds to the inner modes.<sup>36</sup> From the eigenvalues  $\eta_{nl}^S$  and  $\eta_{nl}^T$ , as shown in Fig. 6, we obtained the angular frequencies  $\omega_l^S$  and  $\omega_l^T$  by Eqs. (3) and (5), respectively, and then we obtained the Raman-shift wave numbers  $\nu_l^S$  and  $\nu_l^T$  in this case of CdS. The Raman-shift wave numbers  $\nu_l^S$  of the spheroidal mode with each angular momentum  $l$  less than  $l=3$  for CdS microcrystal are represented as follows:

$$\nu_0^S = 0.78 \frac{v_t}{dc} \quad (n=0), \quad \nu_0^S = 1.90 \frac{v_t}{dc} \quad (n=1), \quad (6)$$

$$\nu_1^S = 1.17 \frac{v_t}{dc} \quad (n=0), \quad (7)$$

$$\nu_2^S = 0.85 \frac{v_t}{dc} \quad (n=0), \quad (8)$$

$$\nu_3^S = 1.26 \frac{v_t}{dc} \quad (n=0), \quad (9)$$

where  $c$  is the velocity of light. In Eqs. (7)–(9), only the lowest Raman-shift wave numbers with  $n=0$  (the surface modes) for each angular momentum are shown except for angular momentum  $l=0$ . The lowest wave number with  $n=0$  (the surface mode) and the secondary wave number with  $n=1$  (the inner mode) for angular momentum  $l=0$  are given by Eq. (6). The low-frequency Raman band that Duval, Boukenter, and Champagnon have reported for nucleated glass at first<sup>30</sup> corresponds to the lowest-

frequency mode ( $n=0$ ) of the spheroidal mode with  $l=0$  [the former in Eq. (6)], that is, to the surface mode.

Similarly, the lowest Raman-shift wave numbers  $\nu_l^T$  of the torsional mode with  $n=0$  for each angular momentum  $l$  less than 3 are represented by

$$\nu_1^T = 1.83 \frac{v_t}{dc} \quad (n=0), \quad (10)$$

$$\nu_2^T = 0.80 \frac{v_t}{dc} \quad (n=0), \quad (11)$$

$$\nu_3^T = 1.23 \frac{v_t}{dc} \quad (n=0). \quad (12)$$

The Raman-shift wave numbers of torsional modes with  $n=0$  for  $l=1$  and  $l=2$ , as given by Eqs. (10) and (11), are compatible with the results that have been reported already.<sup>34</sup> From the expressions of Eqs. (6)–(12), we obtain that the Raman-shift wave numbers of both modes are proportional to the sound velocities and to the inverse microcrystal diameters. The trend of this theoretical size dependence is compatible with the result of the observation of the peak frequency as a function of the inverse microcrystal diameter.

### C. Selection rules, polarization properties and their application to the present experiment, and comparison between theory and experiment

In addition to the calculated results derived from Lamb's theory, we also tried to analyze our experimental results considering selection rules and polarization properties. As described in the previous paragraph, the displacement vector  $\mathbf{D}_S$  of the spheroidal mode is obtained by introducing the scalar potential  $\phi_S$  and the vector potential  $\mathbf{A} = (r\psi_V, 0, 0)$ . In these expressions,  $\phi_S$  is the scalar potential which is a solution of the Helmholtz wave equation and it is proportional to the spherical harmonic  $Y_{lm}(\theta, \phi)$ . Similarly,  $\psi_V$  is proportional to the spherical harmonic  $Y_{lm}(\theta, \phi)$ . Using these potentials, the displacement vector  $\mathbf{D}_S$  of the spheroidal mode can be represented as

$$\mathbf{D}_S = \nabla \phi_S + \nabla \times \nabla \times \mathbf{A}. \quad (13)$$

On the other hand, the displacement vector  $\mathbf{D}_T$  of the torsional mode is obtained from the vector potential  $\mathbf{A}$  and it can be represented as

$$\mathbf{D}_T = \nabla \times \mathbf{A}. \quad (14)$$

The parity of the scalar functions  $\phi_S$  and  $\psi_V$  is equal to that of the spherical harmonic  $Y_{lm}(\theta, \phi)$  because the scalar functions  $\phi_S$  and  $\psi_V$  are proportional to this spherical harmonic. Furthermore, the parity of the spherical harmonic  $Y_{lm}(\theta, \phi)$  is equal to the parity of the angular momentum  $l$ . From Eqs. (13) and (14), we obtain that the parity of the vibrational wave function (of the displacement vector  $\mathbf{D}$ ) for the spheroidal mode is equal to that of the scalar functions  $\phi_S$  and  $\psi_V$ , and the parity of the vibrational wave function for the torsional mode is opposite that of the scalar function  $\psi_V$ . Consequently, the spheroidal modes for even  $l$  are Raman-active modes, and

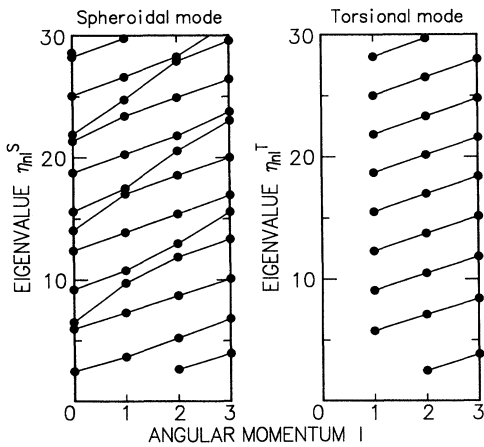


FIG. 6. Dispersion relations of the spheroidal modes and the torsional modes for CdS microcrystal as solved in the eigenvalue equations (2) and (4).

the torsional modes for odd  $l$  are Raman-active modes.<sup>34</sup> Furthermore, only the Raman scattering of the spheroidal mode with  $l=0$  is expected to be perfectly polarized and that of all other modes is expected to be partially depolarized, because only the spheroidal mode with  $l=0$  is perfectly symmetric.

In the reduced spectra of polarized scattering for the samples with  $d=16.1$  and  $11.8$  nm, the peaks were observed at  $7.4$  and  $9.0$   $\text{cm}^{-1}$ , respectively. In the reduced spectrum of polarized scattering for the sample with  $d=9.3$  nm, the lower-frequency peak was observed at  $6.0$   $\text{cm}^{-1}$  and the higher-frequency peak was observed at  $11.0$   $\text{cm}^{-1}$ . In the reduced spectrum of polarized scattering for the sample with  $d=7.5$  nm, the lower-frequency peak was observed at  $6.6$   $\text{cm}^{-1}$  and higher-frequency peak was observed at  $14.5$   $\text{cm}^{-1}$ . The peaks observed in the polarized spectra could not be observed in the depolarized spectra for the samples with  $d=16.1$ ,  $11.8$ , and  $9.3$  nm. However, in the depolarized spectra for the sample with  $d=7.5$  nm, a distinct peak was observed at  $7.1$   $\text{cm}^{-1}$ , and its peak wave number was found to be close to the peak wave number of the lower-frequency peak observed in the polarized spectrum, but some discrepancies are observed between these peak wave numbers in the polarized and depolarized spectra. We believe that the origin of the peak in the depolarized spectrum is different from that of the lower-frequency peak in the polarized spectrum, and both of two peaks observed in the polarized spectrum also could not be observed in the depolarized spectrum for the sample with  $d=7.5$  nm. This characteristic polarization property means that the observed modes in the polarized spectra are perfectly polarized. Since only the Raman scattering of the spheroidal mode with  $l=0$  is expected to be perfectly polarized, the observed peaks in the polarized spectra originate from the spheroidal mode with  $l=0$ . The shapes of CdS microcrystals in these cases are almost spherical, because the spheroidal mode with  $l=0$  is perfectly polarized only if the microcrystals are spherical. These results are compatible with the results of the direct observation of these CdS microcrystals by the transmission electron microscope. In the polarized scattering spectra for the samples with  $d=9.3$  and  $7.5$  nm, the lower-frequency peak originates from the lowest-order eigenstate ( $n=0$ ) of the spheroidal mode with  $l=0$ , and the higher-frequency peak originates from the higher-order eigenstate ( $n=1$ ) of the spheroidal mode with  $l=0$ . In other words, the lower-frequency peak corresponds to the surface mode among the spheroidal mode with  $l=0$ , and the higher-frequency peak corresponds to the inner mode among the spheroidal mode with  $l=0$ . The peaks in the polarized spectra for the samples with  $d=16.1$  and  $11.8$  nm also originate from the higher-order eigenstate ( $n=1$ ) of the spheroidal mode with  $l=0$ , that is, the inner mode among the spheroidal mode with  $l=0$ . As shown in Fig. 5(a), the agreement of the experimental peak positions obtained from the reduced polarized spectra (the solid circles) and the calculated Raman-shift wave number of the spheroidal modes with  $l=0$  (the solid lines) is fairly good. As shown in Fig. 5(b), the wave numbers of the higher-frequency peaks observed in the polarized spectra are

close to the calculated Raman-shift wave number of the torsional mode with  $l=1$  (the solid line); however, the torsional mode with  $l=1$  is partially depolarized. Furthermore, the lower-peak wave numbers observed in the polarized spectra are close to the calculated Raman-shift wave numbers of the torsional mode with  $l=2$  (the dashed line); however, the torsional mode with  $l=2$  is not Raman active. Therefore, we have to conclude that the observed peaks in the polarized spectra originate from the spheroidal mode with  $l=0$ . The reason that only the tail part of the peak was observed in the polarized scattering spectra for the sample with  $d=25.2$  nm is that the Raman-shift wave number of the spheroidal mode with  $l=0$  is lower than  $5$   $\text{cm}^{-1}$ . Similarly, the reasons that the lowest-order eigenstates ( $n=0$ ) of the spheroidal mode with  $l=0$  cannot be observed for the samples with  $d=16.1$  and  $11.8$  nm are that their Raman-shift wave numbers are lower than  $5$   $\text{cm}^{-1}$ .

Next, we consider the origin of the observed peak in the depolarized spectrum for the sample with  $d=7.5$  nm. As shown in Fig. 5(a), the peak wave number of the observed peak in the depolarized spectrum (solid triangle) is close to the calculated results of the spheroidal modes with  $l=0$  (solid line) and  $l=2$  (dotted line). As shown in Fig. 5(b), it is also close to the calculated results of the torsional mode with  $l=2$  (dashed line). However, since the spheroidal mode with  $l=0$  is perfectly polarized, the spheroidal mode with  $l=0$  cannot be observed in the depolarized spectrum. From the selection rules of the parity of displacement vector (vibrational wave function), the torsional mode with  $l=2$  is not Raman active. Therefore, we have to conclude that the observed peak in the depolarized spectrum originates from the spheroidal mode with  $l=2$  ( $n=0$ ). Since the theoretical results show that the wave numbers of the spheroidal modes with  $l=0$  ( $n=0$ ) and  $l=2$  ( $n=0$ ) have almost the same values as that shown in Fig. 5(a), a peak wave number in the depolarized spectrum is considered to be close to the peak wave number of the lower-frequency peak in the polarized spectrum for the sample with  $d=7.5$  nm. Raman scattering from the samples with  $d=25.2$ ,  $16.1$ ,  $11.8$ , and  $9.3$  nm could not be observed in the depolarized spectra, since the Raman-shift wave numbers of the spheroidal mode with  $l=2$  ( $n=0$ ) are lower than  $5$   $\text{cm}^{-1}$ .

#### D. Comments on the applicability of Lamb's theory

As we have shown above, Lamb's theory could explain well the observed size dependence of Raman peak frequencies. Lamb's theory assumed that the microcrystal is a homogeneous elastic body. This assumption is reasonable if the microcrystal is large enough and does not have large anisotropy in its elastic constants. As shown in Fig. 5, the good agreement between the observed peak frequencies and the peak frequencies calculated from Lamb's theory may indicate that this assumption is reasonable in the present size ranges (larger than  $d=7.5$  nm) for CdS microcrystals. However, if the microcrystal size is much smaller than present CdS microcrystals in our measurement, this continuum assumption may not be reasonable.

## V. SUMMARY AND CONCLUSIONS

We measured the polarization properties of low-frequency Raman-scattering spectra of CdS microcrystals embedded in a germanium dioxide glass matrix. We found that the peaks observed in the reduced polarized spectra were not observed in the reduced depolarized spectra, but a different peak was observed in the reduced depolarized spectra. The peak wave numbers obtained from polarized and depolarized spectra were found to be proportional to the inverse microcrystal diameters. It was shown that these experimental results agree well with the calculated results based on Lamb's theory, which describes the free vibration of a homogeneous spherical elastic body, and that this low-frequency Raman scattering that we observed originates from the confined acous-

tic vibrations of a spherical CdS microcrystal. From a consideration of the theoretically calculated results, the experimentally obtained polarization properties, and also the selection rules related to the parity of the vibrational displacement, we could assign the observed polarized Raman scattering to the spheroidal mode with  $l=0$ , and also assign the observed depolarized Raman scattering to the spheroidal mode with  $l=2$ .

## ACKNOWLEDGMENT

We thank the Ministry of Education, Science and Culture for financial support under Grant-in-Aid Nos. 04230104, 04230101, and 04230207 for Scientific Research.

- 
- <sup>1</sup>T. Itoh, Y. Iwabuchi, and M. Kataoka, *Phys. Status Solidi B* **145**, 567 (1988).  
<sup>2</sup>T. Itoh, Y. Iwabuchi, and T. Kirihara, *Phys. Status Solidi B* **146**, 531 (1988).  
<sup>3</sup>T. Arai, H. Fujimura, I. Umezu, T. Ogawa, and A. Fujii, *Jpn. J. Appl. Phys.* **28**, 484 (1989).  
<sup>4</sup>T. Inokuma, T. Arai, and M. Ishikawa, *Phys. Rev. B* **42**, 11 093 (1990).  
<sup>5</sup>A. Nakamura, H. Yamada, and T. Tokizaki, *Phys. Rev. B* **40**, 8585 (1989).  
<sup>6</sup>A. I. Ekimov, A. L. Efros, and A. A. Onushenko, *Solid State Commun.* **56**, 921 (1985).  
<sup>7</sup>N. F. Borrelli, D. W. Hall, H. J. Holland, and D. W. Smith, *J. Appl. Phys.* **61**, 5399 (1987).  
<sup>8</sup>S. Hayashi, M. Fujii, and K. Yamamoto, *Jpn. J. Appl. Phys.* **28**, L1464 (1989).  
<sup>9</sup>R. K. Jain and R. C. Lind, *J. Opt. Soc. Am.* **73**, 647 (1983).  
<sup>10</sup>J. P. Zheng and H. S. Kwok, *Appl. Phys. Lett.* **54**, 1 (1989).  
<sup>11</sup>A. L. Efros and A. L. Efros, *Fiz. Tekh. Poluprovodn.* **16**, 1209 (1982) [*Sov. Phys. Semicond.* **16**, 772 (1982)].  
<sup>12</sup>L. E. Brus, *J. Chem. Phys.* **80**, 4403 (1984).  
<sup>13</sup>Y. Kayanuma, *Solid State Commun.* **59**, 405 (1986).  
<sup>14</sup>Y. Kayanuma, *Phys. Rev. B* **38**, 9797 (1988).  
<sup>15</sup>S. V. Nair, S. Sinha, and K. C. Rustagi, *Phys. Rev. B* **35**, 4098 (1987).  
<sup>16</sup>S. Schmitt-Rink, D. A. B. Miller, and D. S. Chemla, *Phys. Rev. B* **35**, 8113 (1987).  
<sup>17</sup>E. Hanamura, *Phys. Rev. B* **38**, 1228 (1988).  
<sup>18</sup>H. Richter, Z. P. Wang, and L. Ley, *Solid State Commun.* **39**, 625 (1981).  
<sup>19</sup>I. H. Campbell and P. M. Faucher, *Solid State Commun.* **58**, 739 (1986).  
<sup>20</sup>K. K. Tiong, P. M. Amirtharaj, F. H. Pollak, and D. E. Aspnes, *Appl. Phys. Lett.* **44**, 122 (1984).  
<sup>21</sup>M. Fujii, S. Hayashi, and K. Yamamoto, *Appl. Phys. Lett.* **57**, 2692 (1990).  
<sup>22</sup>M. Fujii, S. Hayashi, and K. Yamamoto, *Jpn. J. Appl. Phys.* **30**, 687 (1991).  
<sup>23</sup>A. Tanaka, S. Onari, and T. Arai, *Phys. Rev. B* **45**, 6587 (1992).  
<sup>24</sup>S. Hayashi and R. Ruppin, *J. Phys. C* **18**, 2583 (1985).  
<sup>25</sup>F. Zhou, Y. Sun, and J. Pan, *J. Lumin.* **40&41**, 739 (1988).  
<sup>26</sup>S. Hayashi and H. Kanamori, *Phys. Rev. B* **26**, 7079 (1982).  
<sup>27</sup>T. Okada, T. Iwaki, H. Kasahara, and K. Yamamoto, *J. Phys. Soc. Jpn.* **54**, 1173 (1985).  
<sup>28</sup>S. Hayashi and H. Abe, *Jpn. J. Appl. Phys.* **23**, L824 (1984).  
<sup>29</sup>Z. Iqbal, S. Veprek, A. P. Webb, and P. Capezzuto, *Solid State Commun.* **37**, 993 (1981).  
<sup>30</sup>E. Duval, A. Boukenter, and B. Champagnon, *Phys. Rev. Lett.* **56**, 2052 (1986).  
<sup>31</sup>V. K. Malinovsky, V. N. Novikov, and A. P. Sokolov, *Solid State Commun.* **67**, 725 (1988).  
<sup>32</sup>N. N. Ovsyuk, E. B. Gorokhov, V. V. Grishchenko, and A. P. Shebanin, *Pis'ma Zh. Eksp. Teor. Fiz.* **47**, 248 (1988) [*JETP Lett.* **47**, 298 (1988)].  
<sup>33</sup>G. Mariotto, M. Montagna, G. Viliani, E. Duval, S. Lefrant, E. Rzepka, and C. Mai, *Europhys. Lett.* **6**, 239 (1988).  
<sup>34</sup>M. Fujii, S. Hayashi, and K. Yamamoto, *Phys. Rev. B* **44**, 6243 (1991).  
<sup>35</sup>H. Lamb, *Proc. Lond. Math. Soc.* **13**, 189 (1982).  
<sup>36</sup>A. Tamura, K. Higeta, and T. Ichinokawa, *J. Phys. C* **15**, 4975 (1982).  
<sup>37</sup>A. Tamura and T. Ichinokawa, *J. Phys. C* **16**, 4779 (1983).  
<sup>38</sup>N. Nishiguchi and T. Sakuma, *Solid State Commun.* **38**, 1073 (1981).  
<sup>39</sup>D. Gerlich, *J. Phys. Chem. Solids* **28**, 2575 (1967).